Mammalian Heart Renewal by Preexisting Cardiomyocytes

Samuel E. Senyo[1], **Matthew L. Steinhauser**[1], **Christie L. Pizzimenti**[1], **Vicky K. Yang**[1], **Lei Cai**[1], **Mei Wang**[4,5], **Ting-Di Wu**[2,3], **Jean-Luc Guerquin-Kern**[2,3], **Claude P. Lechene**[4,5], and **Richard T. Lee**[1,6]

[1]Cardiovascular Division, Department of Medicine, Brigham and Women's Hospital and Harvard Medical School

[2]INSERM, U.759, F-91405 Orsay (France)

[3]Institut Curie, Laboratoire de Microscopie Ionique, F-91405 Orsay (France)

[4]National Resource for Imaging Mass Spectrometry

[5]Genetics Division, Department of Medicine, Brigham and Women's Hospital and Harvard Medical School

[6]Harvard Stem Cell Institute

Although recent studies have revealed that heart cells are generated in adult mammals, the frequency and source of new heart cells is unclear. Some studies suggest a high rate of stem cell activity with differentiation of progenitors to cardiomyocytes[1]. Other studies suggest that new cardiomyocytes are born at a very low rate[2,3,4], and that they may be derived from division of pre-existing cardiomyocytes. Thus, the origin of cardiomyocytes in adult mammals remains unknown. Here we combined two different pulse-chase approaches -- genetic fate-mapping with stable isotope labeling and Multi-isotope Imaging Mass Spectrometry (MIMS). We show that genesis of cardiomyocytes occurs at a low rate by division of pre-existing cardiomyocytes during normal aging, a process that increases by four-fold adjacent to areas of myocardial injury. Cell cycle activity during normal aging and after injury led to polyploidy and multinucleation, but also to new diploid, mononucleated cardiomyocytes. These data reveal pre-existing cardiomyocytes as the dominant source of cardiomyocyte replacement in normal mammalian myocardial homeostasis as well as after myocardial injury.

Despite intensive research, fundamental aspects of the mammalian heart's capacity for self-renewal are actively debated[5,6]. Estimates of cardiomyocyte turnover range from less than 1% per year[2,3,4] to more than 40% per year[7]. Turnover has been reported to either decrease[3]

or increase with age[7], while the source of new cardiomyocytes has been attributed to both division of existing myocytes[8] and to progenitors residing within the heart[9] or in exogenous niches such as bone marrow[10]. Controversy persists regarding the plasticity of the adult heart in part due to methodological challenges associated with studying slowly replenished tissues. Toxicity attributed to radiolabeled thymidine[11] and halogenated nucleotide analogues[12] limits the duration of labeling and may produce direct biological effects. Tissue autofluorescence can reduce the sensitivity and specificity of immunofluorescent methods of detecting cell cycle activity[5,13], including as cell cycle markers or incorporation of halogenated nucleotide analogues. The challenge of measuring cardiomyocyte turnover is further compounded by the faster rate of turnover of cardiac stromal cells relative to cardiomyocytes[14].

We used Multi-isotope Imaging Mass Spectrometry (MIMS) to study cardiomyocyte turnover and to determine whether new cardiomyocytes are derived from preexisting myocytes or from a progenitor pool (Fig 1a). MIMS uses ion microscopy and mass spectrometry to generate high resolution quantitative mass images and localize stable isotope reporters in domains smaller than one micron cubed[15,16,17]. MIMS generates ^{14}N quantitative mass images by measuring the atomic composition of the sample surface with a lateral resolution of under 50nm and a depth resolution of a few atomic layers. Cardiomyocyte cell borders and intracellular organelles were easily resolved (Fig 1b). Regions of interest can be analyzed at higher resolution, demonstrating cardiomyocyte-specific subcellular ultrastructure, including sarcomeres (Fig 1c, Supplemental Fig 1a). In all subsequent analyses, cardiomyocyte nuclei were identified by their location within sarcomere-containing cells, distinguishing them from adjacent stromal cells.

An immense advantage of MIMS is the detection of nonradioactive stable isotope tracers. As an integral part of animate and inanimate matter, they do not alter biochemical reactions and are not harmful to the organism[18]. MIMS localizes stable isotope tracers by simultaneously quantifying multiple masses from each analyzed domain; this enables the generation of a quantitative ratio image of two stable isotopes of the same element[15]. The incorporation of a tracer tagged with the rare stable isotope of nitrogen (^{15}N) is detectable with high precision by an increase in ^{15}N:^{14}N above the natural ratio (0.37%). Nuclear incorporation of ^{15}N-thymidine is evident in cells having divided during a one-week labeling period, as observed in the small intestinal epithelium, which turns over completely in 3–5 days[16] (Fig 1d); in contrast, ^{15}N-thymidine labeled cells are rarely observed in the heart (Fig 1e) after 1 week of labeling. In subsequent studies, small intestine was used as a positive control to confirm label delivery.

To evaluate for an age-related change in cell cycle activity, we administered ^{15}N-thymidine for 8 weeks to three age groups of C57BL6 mice starting at day-4 (neonate), at 10-weeks (young adult) and at 22-months (old adult) (Supplemental Fig 2). We then performed MIMS analysis (Fig 2a, b, Supplemental Fig 3). In the neonatal group, 56% (±3% s.e.m., n=3 mice) of cardiomyocytes demonstrated ^{15}N nuclear labeling, consistent with the well-accepted occurrence of cardiomyocyte DNA synthesis during post-natal development[19]. We observed a marked decline in the frequency of ^{15}N-labeled cardiomyocyte nuclei (^{15}N$^+$CM) in the young adult (neonate= 1.00% ^{15}N$^+$CM/day ±0.05 s.e.m. vs young

adult=0.015% ^{15}N$^+$CM/day ±0.003 s.e.m., n=3 mice/group, p<0.001) (Fig 2a, c; Supplemental Fig 3). We found a further reduction in cardiomyocyte DNA synthesis in old mice (young adult=0.015% ^{15}N$^+$CM/day ±0.003 s.e.m. vs. old adult=0.007 % ^{15}N$^+$CM/day ±0.002 s.e.m., n=3/group, p<0.05) (Fig 2c). The observed pattern of nuclear ^{15}N-labeling in cardiomyocytes is consistent with the known chromatin distribution pattern in cardiomyocytes[20] (Supplemental Fig 1b) and was measured at levels that could not be explained by DNA repair (Supplemental Fig 4). Extrapolating DNA synthesis measured in cardiomyocytes over 8 weeks yields a yearly rate of 5.5% in the young adult and 2.6% in the old mice. Given that cardiomyocytes are known to undergo DNA replication without completing the cell cycle[19,21,22], these calculations represent the upper limit of cardiomyocyte generation under normal homeostatic conditions, indicating a low rate of cardiogenesis.

To test whether cell cycle activity occurred in preexisting cardiomyocytes or was dependent on a progenitor pool, we performed ^{15}N-thymidine labeling of double-transgenic MerCreMer/ZEG mice, previously developed for genetic lineage mapping (Fig 3a)[23,24]. MerCreMer/ZEG cardiomyocytes irreversibly express green fluorescent protein (GFP) after treatment with 4OH-tamoxifen, allowing pulse labeling of existing cardiomyocytes with a reproducible efficiency of approximately 80%. Although some have reported rare GFP expression by non-cardiomyocytes with this approach[25], we did not detect GFP expression in interstitial cells isolated from MerCreMer/ZEG hearts nor did we detect GFP expression by Sca1 or ckit-expressing progenitors in histological sections (Supplemental Fig 5). Thus, during a chase period, cardiomyocytes generated from progenitors should be GFP$^-$, whereas cardiomyocytes arising from preexisting cardiomyocytes should express GFP at a frequency similar to the background rate induced by 4OH-tamoxifen. We administered 4OH-tamoxifen for two weeks to 8 wk-old mice (n=4); during a subsequent 10-week chase, mice received ^{15}N-thymidine via osmotic minipump (20μg/h). With MIMS analysis, we identified 35 ^{15}N-labeled cardiomyocyte nuclei (of 4190 analyzed) over 10 weeks, yielding a projected yearly rate of cardiomyocyte DNA replication of 4.4%. Extrapolating from prior reports of high stem cell-dependent cardiomyocyte turnover[7], we had anticipated detecting >320 cardiomyocytes entering the cell cycle; these results exclude such a high rate of turnover (expected ^{15}N$^+$ cardiomyocytes=321; observed=35; Fisher's exact<0.0001). Immunofluorescent staining for GFP was performed on adjacent sections and an observer unaware of MIMS analysis results assessed GFP status. Of ^{15}N$^+$ cardiomyocytes, 77% expressed GFP, a frequency essentially identical to that of surrounding ^{15}N$^-$ cardiomyocytes (^{15}N$^+$ CM, 77% vs ^{15}N$^-$ cardiomyocytes, 84%; Fisher's exact=n.s.) (Table 1). If new cardiomyocytes were derived from progenitors, ^{15}N$^+$ cardiomyocytes would have been GFP$^-$ (expected=0/35; observed=27/35, Fisher's exact<0.0001). These data reveal that ^{15}N-labeled cardiomyocytes resulted from DNA synthesis by preexisting cardiomyocytes and exclude a substantial contribution from stem cells to cardiomyocyte replacement in the uninjured heart.

Cardiomyocytes can undergo DNA replication without completing the cell cycle. Although multinucleation and polyploidization occur during early post-natal development and in response to myocardial stress[2,19], we considered the possibility these processes could

account for $^{15}N^+$ cardiomyocytes in the uninjured adult mouse. We performed fluorescent *in situ* hybridization in adjacent sections to assess the ploidy state of each $^{15}N^+$ cardiomyocyte and surrounding $^{15}N^-$ cardiomyocytes, and an observer unaware of the results of MIMS analysis identified fluorescently-labeled chromosomes (Supplemental Fig 6). Although we found $^{15}N^+$ cardiomyocytes that were polyploid (4n or greater), we observed a higher frequency of diploid nuclei in the $^{15}N^+$ pool compared to surrounding $^{15}N^-$ cardiomyocytes ($^{15}N^+$ diploid:polyploid = 22:12 vs $^{15}N^-$ diploid:polyploid = 9:56, Fisher's exact p<0.0001), consistent with ongoing cell division. We then assessed each cell for multinucleation using serial 0.5μm sections adjacent to the section used for MIMS analysis (Supplemental Fig 6). We observed that 49% of $^{15}N^+$ cardiomyocytes were mononucleated, in contrast to a frequency of 24% for surrounding $^{15}N^-$ cardiomyocytes (Fisher's exact p<0.01), also consistent with cell division. The majority of cardiomyocyte DNA synthesis occurred in polyploid and/or multinucleated cardiomyocytes as might be expected with a physiologic hypertrophic response and thus unlikely to indicate cardiomyocyte division; however, 17% (6 of 35 $^{15}N^+$ CM) were diploid and mononucleated, consistent with newly generated cardiomyocytes (Supplemental Fig 7). The mononucleated, diploid, $^{15}N^+$ cardiomyocytes were also predominantly GFP$^+$ (5 of 6 = 83% vs. 82% background frequency, p=n.s.), suggesting that they arose from preexisting cardiomyocytes at a slow annual rate of 0.76% (n=6 of 4190 over 10 weeks).

We next used MIMS and genetic fate mapping to study myocardial injury. Cardiomyocyte GFP labeling was induced in MerCreMer/ZEG mice with 4OH-tamoxifen. Mice then underwent experimental myocardial infarction or sham surgery followed by continuous labeling with ^{15}N-thymidine for 8wks. The frequency of ^{15}N-labeled cardiomyocytes in sham-operated mice was similar to prior experiments in unoperated mice (yearly projected rates: sham=6.8%; unoperated=4.4%), but increased significantly adjacent to infarcted myocardium (total $^{15}N^+$ cardiomyocyte nuclei: MI=23.0% vs sham=1.1%, Fig 4a–b, Supplemental Fig 8). We examined GFP expression, nucleation and ploidy status of ^{15}N-labeled cardiomyocytes and surrounding unlabeled cardiomyocytes. We found a significant dilution of the GFP$^+$ cardiomyocyte pool at the border region as previously shown[23,24] (67% vs. 79%, p<0.05, Table 2, Supplemental Fig 9); however, $^{15}N^+$ myocytes demonstrated a similar frequency of GFP expression compared to unlabeled myocytes (71% vs. 67%, Fisher's exact=n.s.), suggesting that DNA synthesis was primarily occurring in pre-existing cardiomyocytes. Of ^{15}N-labeled cardiomyocytes, approximately 14% were mononucleated and diploid consistent with division of pre-existing cardiomyocytes (Supplemental Fig 6, 7). We observed higher DNA content (>2N) in the remaining cardiomyocytes as expected with compensatory hypertrophy after injury. Thus, in the 8wks after myocardial infarction, approximately 3.2% of the cardiomyocytes adjacent to the infarct had unambiguously undergone division (total $^{15}N^+ \times$ mononucleated diploid fraction = 23% $\times$ 0.14 = 3.2%). The low rate of cardiomyocyte cell cycle completion is further supported by the absence of detectable Aurora B Kinase, a transiently expressed cytokinesis marker, which was detected in rapidly proliferating small intestinal cells but not in cardiomyocytes (Supplemental Fig 10). We also considered the possibility that a subset of $^{15}N^+$ myocytes that were multinucleated and/or polyploid resulted from division followed by additional rounds of DNA synthesis without division. However, quantitative analysis of the $^{15}N^+$ population did

not identify a subpopulation that had accumulated additional ^{15}N-label as would be expected in such a scenario (Supplemental Fig 11). Together, these data suggest that adult cardiomyocytes retain some capacity to reenter the cell cycle, but that the majority of DNA synthesis after injury occurs in preexisting cardiomyocytes without completion of cell division.

If dilution of the GFP$^+$ cardiomyocyte pool cannot be attributed to division and differentiation of endogenous progenitors, do these data exclude a role for progenitors in the adult mammalian heart? These data could be explained by preferential loss of GFP$^+$ cardiomyocytes after injury, a process that we have previously considered but for which we have not found supporting evidence[23]. Such an explanation excludes a role for endogenous progenitors in cardiac repair and would be consistent with data emerging from lower vertebrates[8,26] and the neonatal mouse[27] in which preexisting cardiomyocytes are the cellular source for cardiomyocyte repletion. A second possibility to explain the dilution of the GFP$^+$ cardiomyocyte pool is that injury stimulates progenitor differentiation without division; inevitably, this would lead to exhaustion of the progenitor pool, which if true could explain the limited regenerative potential of the adult mammalian heart.

In summary, this study demonstrates birth of cardiomyocytes from preexisting cardiomyocytes at a projected rate of approximately 0.76%/year (^{15}N$^+$ annual rate $\times$ mononucleated diploid fraction = 4.4% $\times$ 0.17) in the young adult mouse under normal homeostatic conditions, a rate that declines with age but increases by approximately four-fold after myocardial injury in the border region. This study shows that cardiac progenitors do not play a significant role in myocardial homeostasis in mammals and suggests that their role after injury is also limited.

Online Methods

Mice

All experiments were conducted in accordance with the *Guide for the Use and Care of Laboratory Animals* and approved by the Harvard Medical School Standing Committee on Animals. C57Bl/6 male mice were obtained from Charles River.

We generated double transgenic Mer-CreMer-ZEG male mice by crossbreeding cardiomyocyte-specific MerCreMer mice and ZEG mice (Jackson Laboratory). β-galactosidase-GFP is under the control of a cytomegalovirus (CMV) enhancer/chicken actin promoter (*Actb*); the background strain was C57BL/6J (N7). The background strain of the MerCreMer mice was C57Bl/6SV129. Genotyping was performed by PCR on tail DNA using the following primers: MerCreMer forward: 5′-GTCTGAC TAGGTGTCCTTCT-3′; MerCreMer backward: 5′-CGTCCTCCTGCTGGTA TAG-3′; ZEG forward: 5′-AAGTTCATCTGCACCACCG-3′; *ZEG* backward: 5′-TCCTTGAAGAAGATGGTGCG-3′; ZEG control forward: 5′-CTAGGCCA CAGAATTGAAAGATCT-3′; and ZEG control backward: 5′-GTAGGTG GAAATTCTAGCATCATCC-3′. To induce Cre recombination and GFP labeling in cardiomyocytes, we injected 4-OH-tamoxifen (provided by a generous gift from Laboratoires Besins), dissolved in peanut oil (Sigma) at a concentration of 5 mg/ml,

intraperitoneally into 8-week-old MerCreMer-ZEG mice daily at a dosage of 0.5 mg/day for 14 days.

Experimental myocardial infarction

Mice were subjected to experimental myocardial infarction as described. Surgeries were performed by a single operator with more than 20 years of experience in the performance of coronary ligation in rodents. In brief, the left coronary artery was permanently ligated approximately 2 mm below the left atrial appendage. For sham operations, the thoracic cavity was opened and the heart exposed, but no intramyocardial sutures were placed. ^{15}N-thymidine (Cambridge Isotopes) was administered at a rate of 20μg/hr via osmotic minipump (Alzet), implanted subcutaneously at the time of experimental myocardial infarction after a single intraperitoneal bolus dose of 500μg.

MIMS data acquisition

The factory prototype of the NanoSIMS50 as well as a standard NanoSIMS 50 and a large radius NanoSIMS 50L (Cameca, Gennevilliers, France) was used for MIMS analysis as previously described[15]. A focused beam of Cs+ ions was used to sputter a few atomic layers and generate secondary ions from the left ventricular free wall of heart section samples. The Cs+ primary ions were scanned over a raster pattern of either 256×256 pixels or 512×512 pixels. At each pixel location, the secondary ion intensities for $^{12}C^-$, $^{13}C^-$, $^{12}C^{14}N^-$ and $^{12}C^{15}N^-$were recorded in parallel from the same sputtered volume. The detection of nitrogen requires the use of cluster ions $^{12}C^{14}N^-$ and $^{12}C^{15}N^-$ for ^{14}N and ^{15}N, respectively, due to the low ionization efficiency of nitrogen as N^-.

MIMS data analysis

From a single field image acquisition, we first extracted four image files: the four original quantitative mass images (QMIs; ^{12}C, ^{13}C, $^{12}C^{14}N$, $^{12}C^{15}N$) and the two ratio images ($^{13}C/^{12}C$ and $^{12}C^{15}N/^{12}C^{14}N$), derived from the pixel-by-pixel division of the ^{13}C QMI by the ^{12}C QMI and of the $^{12}C^{15}N$ QMI by the $^{12}C^{14}N$ QMI, respectively. We then used a hue saturation intensity transformation (HSI) of the ratio image to map ^{15}N-labeled regions. The hue corresponds to the ratio value, and the intensity at a given hue is an index of statistical reliability.

^{15}N-thymidine labeling

For the neonatal cohort in the aging experiment, labeling was starting at post-natal day 4 with subcutaneous injections of 50μg/g ^{15}N-thymidine (Cambridge Isotopes) every 12h and continued through post-natal week 4. Starting at age 4 wks – and in all other experiments using adult mice – osmotic minipumps (Alzet) were implanted subcutaneously, delivering ^{15}N-thymidine (Cambridge Isotopes) at a rate of 20 μg/hour.

Multinucleation Analysis

Serial adjacent sections (0.5μm) were stained to identify cardiomyocyte borders. A given cardiomyocyte was tracked in the vertical axis by locating it in serial sections. Uninjured hearts were stained using a modified PAS protocol with standard solutions (Electron

Microscopy Services), but with longer incubation times optimized for LR white embedding. Slides were incubated in xylene at 37C, 1 hour, rehydrated through graded alcohols, incubated in periodic acid for two hours, and Schiff's reagent for two nights. Sections were counterstained in hematoxylin and Scott's Bluing for 1 hour each. Injured hearts were stained using a modified Trichrome staining protocol with standard solutions (Fisher Scientific), but with longer incubation times. Slides were incubated in xylene at 37C, 1 hour, rehydrated through graded alcohols, incubated in bouin's fluid at 56C, 1 hour, rinsed in tap water, incubated in weigert's iron hematoxylin stain 1 hour, rinsed in tap water, incubated in scarlet-acid fuchsin solution, 1 hour, rinsed in DI water, incubated in phophotungistic-phophomolybdic acid solution, 30 minutes, incubated in aniline blue stain solution, 30 minutes, and incubated in 1% acetic acid, 20 minutes.

Fluorescent in situ hybridization

Sections were incubated in proteinase K (50ug/ml) at 60C for 15min. After a PBS/MgCl2 (45mM) wash, slides were post-fixed in 4% paraformaldehyde (PBS/MgCl2), dehydrated through graded alcohols. Biotinylated-labeled chromosome Y paint (Star-FISH, Cambio) in hybridization mix was applied to sections, and sealed under glass with rubber cement (note some samples were analyzed with chromosome-18 paint due to product discontinuation of Y-paint). Samples were heated to 90C for 15 min. After an overnight incubation at 37C, slides were washed three times with 50% formamide/2x standard saline citrate at 45C, three washes with 2x standard saline citrate at room temperature, and two washes with 4x standard saline citrate/0.1% Tween at room temperature. Samples were blocked 10 minutes with 4x standard saline citrate/0.1% Tween/ 0.05% milk and incubated for 2 hr in streptavidin-conjugated Alexa Fluor 488 (Invitrogen) prior to washing and mounting. An observer unaware of the MIMS images or ^{15}N-thymidine labeling status of the nuclei assigned ploidy status.

Immunofluorescent staining

Sections were incubated in glycine/tris (50mM glycine/0.05M Tris) at room temperature for 5min. After a brief wash with Tris, sections were incubated with chicken anti-GFP (Abcam), rabbit anti-ckit (Abcam), rat anti-sca1 (Abcam) with fresh 0.1%BSA in TBST (TBS/ 0.1%Tween) overnight at 4C. After a brief wash with TBS, sections were incubated with anti-chicken Alexa Fluor 488 (Invitrogen) prior to TBS wash and mounting. An observer unaware of the MIMS images or ^{15}N-thymidine labeling status of the nuclei assigned GFP status.

Fluorescence Image analysis

We used a custom-written script in IP Lab version 4.0 (Scanalytics) imaging software for serial image acquisition. Tissue sections were auto-imaged using an Olympus IX-70 microscope with a digital charge-coupled device camera (CoolSNAP EZ, Roper Scientific), an automated stage with a piezoelectric objective positioner (Polytec PI, Auburn MA) to compensate for deviations in the z-axis. Images were compressed and stitched into a mosaic using stitching software (Canon Photostitch). Multichannel images were merged in ImageJ prior to stitching.

Statistical analysis

Statistical testing was performed using Prism 3.0 (Graphpad). Results are presented as mean ± s.e.m. and were compared using T-tests (significance was assigned for p<0.05). Data comparing event rates were tested with a Fisher-Exact test.

Supplementary Material

Refer to Web version on PubMed Central for supplementary material.

Acknowledgments

References

1. Hosoda T, et al. Clonality of mouse and human cardiomyogenesis in vivo. Proc Natl Acad Sci U S A. 2009; 106:17169–17174. [PubMed: 19805158]

2. Soonpaa MH, Field LJ. Assessment of cardiomyocyte DNA synthesis in normal and injured adult mouse hearts. Am J Physiol Heart Circ Physiol. 1997; 272:H220–226.

3. Bergmann O, et al. Evidence for cardiomyocyte renewal in humans. Science. 2009; 324:98–102. [PubMed: 19342590]

4. Walsh S, Ponten A, Fleischmann BK, Jovinge S. Cardiomyocyte cell cycle control and growth estimation in vivo--an analysis based on cardiomyocyte nuclei. Cardiovasc Res. 2010; 86:365–373. [PubMed: 20071355]

5. Laflamme MA, Murry CE. Heart regeneration. Nature. 2011; 473:326–335. [PubMed: 21593865]

6. Hosoda T, Rota M, Kajstura J, Leri A, Anversa P. Role of stem cells in cardiovascular biology. J Thromb Haemost. 2011; 9(Suppl 1):151–161. [PubMed: 21781250]

7. Kajstura J, et al. Myocyte turnover in the aging human heart. Circ Res. 2010; 107:1374–1386. [PubMed: 21088285]

8. Kikuchi K, et al. Primary contribution to zebrafish heart regeneration by gata4(+) cardiomyocytes. Nature. 2010; 464:601–605. [PubMed: 20336144]

9. Beltrami AP, et al. Adult cardiac stem cells are multipotent and support myocardial regeneration. Cell. 2003; 114:763–776. [PubMed: 14505575]

10. Orlic D, et al. Bone marrow cells regenerate infarcted myocardium. Nature. 2001; 410:701–705. [PubMed: 11287958]

11. Hu VW, Black GE, Torres-Duarte A, Abramson FP. 3H-thymidine is a defective tool with which to measure rates of DNA synthesis. Faseb J. 2002; 16:1456–1457. [PubMed: 12205046]

12. Wilson A, et al. Hematopoietic stem cells reversibly switch from dormancy to self-renewal during homeostasis and repair. Cell. 2008; 135:1118–1129. [PubMed: 19062086]

13. Laflamme MA, Murry CE. Regenerating the heart. Nat Biotechnol. 2005; 23:845–856. [PubMed: 16003373]

14. Bergmann O, et al. Identification of cardiomyocyte nuclei and assessment of ploidy for the analysis of cell turnover. Exp Cell Res. 2010; 317:188–194. [PubMed: 20828558]

15. Lechene C, et al. High-resolution quantitative imaging of mammalian and bacterial cells using stable isotope mass spectrometry. J Biol. 2006; 5:1–30. [PubMed: 16515716]

16. Steinhauser ML, et al. Multi-isotope imaging mass spectrometry quantifies stem cell division and metabolism. Nature. 2012; 481:516–519. [PubMed: 22246326]

17. Zhang DS, et al. Multi-isotope imaging mass spectrometry reveals slow protein turnover in hair-cell stereocilia. Nature. 2012; 481:520–524. [PubMed: 22246323]

18. Klein PD, Klein ER. Stable isotopes: origins and safety. J Clin Pharmacol. 1986; 26:378–382. [PubMed: 3734125]

19. Li F, Wang X, Capasso JM, Gerdes AM. Rapid transition of cardiac myocytes from hyperplasia to hypertrophy during postnatal development. J Mol Cell Cardiol. 1996; 28:1737–1746. [PubMed: 8877783]

20. Nikolova V, et al. Defects in nuclear structure and function promote dilated cardiomyopathy in lamin A/C-deficient mice. J Clin Invest. 2004; 113:357–369. [PubMed: 14755333]

21. Adler CP, Friedburg H. Myocardial DNA content, ploidy level and cell number in geriatric hearts: post-mortem examinations of human myocardium in old age. J Mol Cell Cardiol. 1986; 18:39–53. [PubMed: 3950970]

22. Katzberg AA, Farmer BB, Harris RA. The predominance of binucleation in isolated rat heart myocytes. Am J Anat. 1977; 149:489–499. [PubMed: 906968]

23. Hsieh PC, et al. Evidence from a genetic fate-mapping study that stem cells refresh adult mammalian cardiomyocytes after injury. Nat Med. 2007; 13:970–974. [PubMed: 17660827]

24. Loffredo FS, Steinhauser ML, Gannon J, Lee RT. Bone marrow-derived cell therapy stimulates endogenous cardiomyocyte progenitors and promotes cardiac repair. Cell Stem Cell. 2011; 8:389–398. [PubMed: 21474103]

25. Dong F, et al. Myocardial CXCR4 expression is required for mesenchymal stem cell mediated repair following acute myocardial infarction. Circulation. 126:314–324. [PubMed: 22685115]

26. Jopling C, et al. Zebrafish heart regeneration occurs by cardiomyocyte dedifferentiation and proliferation. Nature. 2010; 464:606–609. [PubMed: 20336145]

27. Porrello ER, et al. Transient regenerative potential of the neonatal mouse heart. Science. 2011; 331:1078–1080. [PubMed: 21350179]
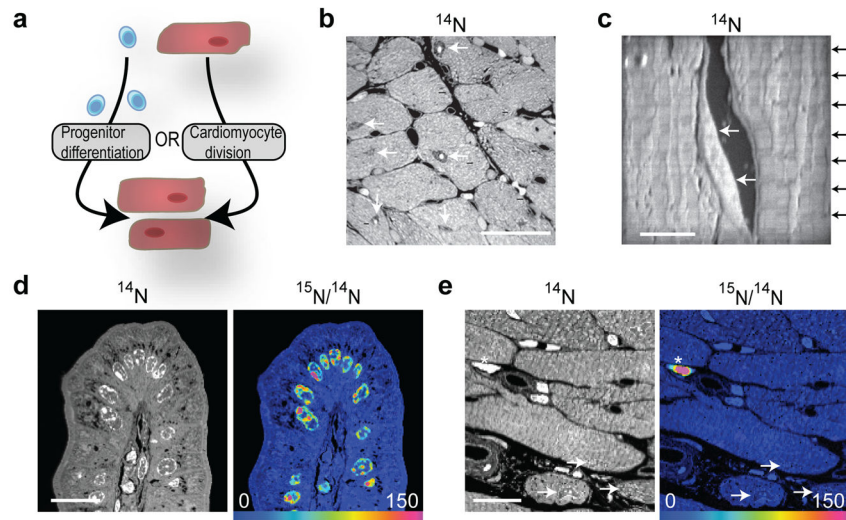
Figure 1. Multi-isotope imaging mass spectrometry (MIMS) to study cardiomyocyte turnover
a) Primary question: are new cardiomyocytes are derived from progenitors or from pre-existing cardiomyocytes?

b) ^{14}N mass image. Subcellular details are evident, including cardiomyocyte nuclei (white arrows). Scale bar = 20μm.

c) MIMS resolves periodic sarcomeres (black arrows) in cardiomyocytes. Non-cardiomyocytes (white arrows) are seen outside cardiomyocyte borders. Scale bar = 5μm.

d) Hue saturation intensity (HSI) ^{15}N:^{14}N image of small intestinal epithelium after ^{15}N-thymidine. The scale ranges from blue, where the ratio is equivalent to natural ratio (0.37%, expressed as 0% above natural ratio), to red, where the ratio is 150% above natural ratio. ^{15}N-labeling is concentrated in nuclei in a pattern resembling chromatin. Scale bar = 15μm.

e) HSI ^{15}N:^{14}N image of heart section (left ventricle). ^{15}N-thymidine administered for 1 wk. Rare ^{15}N-labeled interstitial cells (asterisk). Cardiomyocyte nuclei (white arrows) are unlabeled. Scale bar = 15μm.
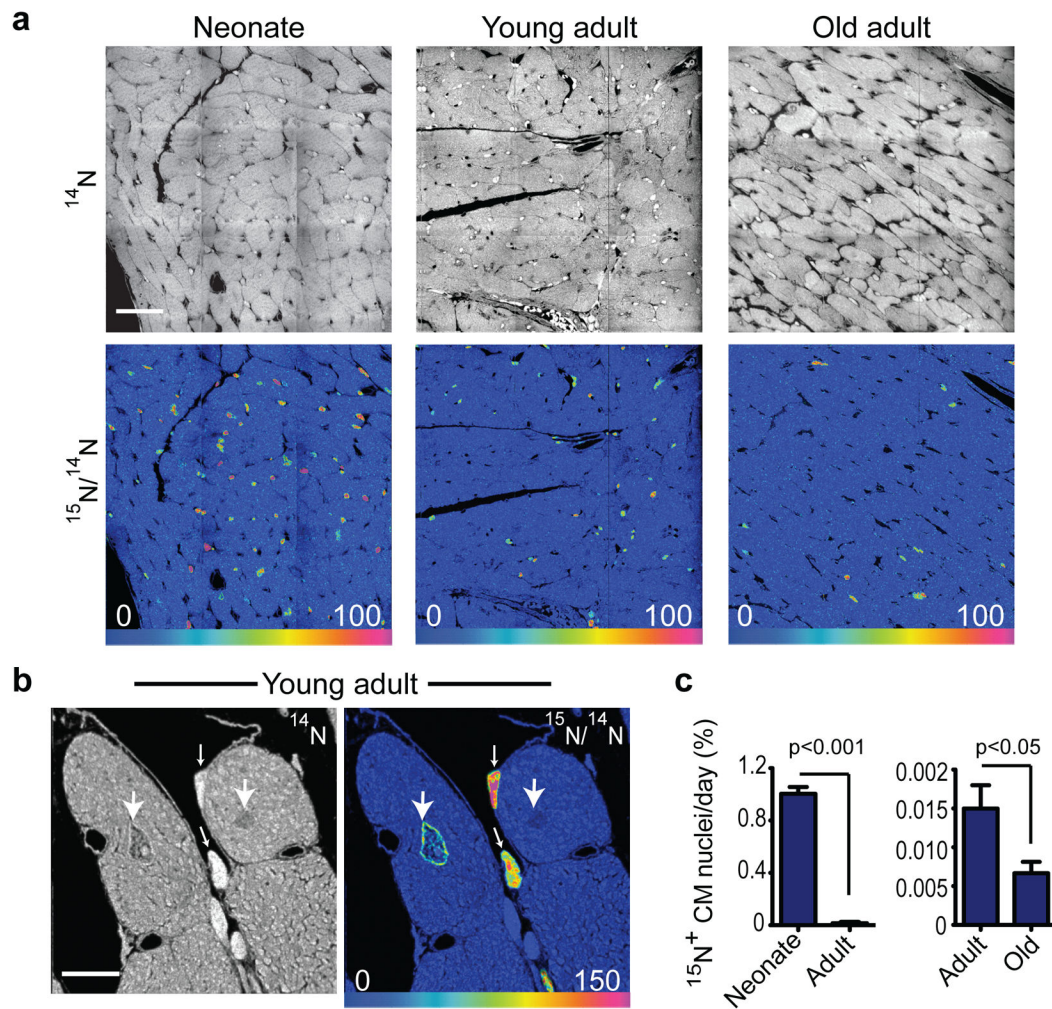
Figure 2. Cardiomyocyte DNA synthesis decreases with age

a) ^{15}N-thymidine administered for 8 wks to mice of different ages: Neonate: starting post-natal day 4, Young adult: starting at 2 mos, Old adult: starting at 22 mos. Top: ^{14}N mass images show histologic details. Bottom: ^{15}N:^{14}N HSI images show ^{15}N-labeled nuclei. Mosaics constructed of 9 tiles, 60μm each. Scale bar = 30μm.

b) High magnification analysis demonstrates cardiomyocyte from the young adult with nuclear ^{15}N-labeling (large arrow), two labeled non-cardiomyocytes (small arrows), and an adjacent unlabeled cardiomyocyte nucleus (medium arrow). Scale bar = 10μm.

c) Age-related decline in cardiomyocyte DNA synthesis. Left: neonate compared to young adult. Right: Scale reduced to compare young adult to old adult (n=3 mice per group). Mean % ± S.E.M.
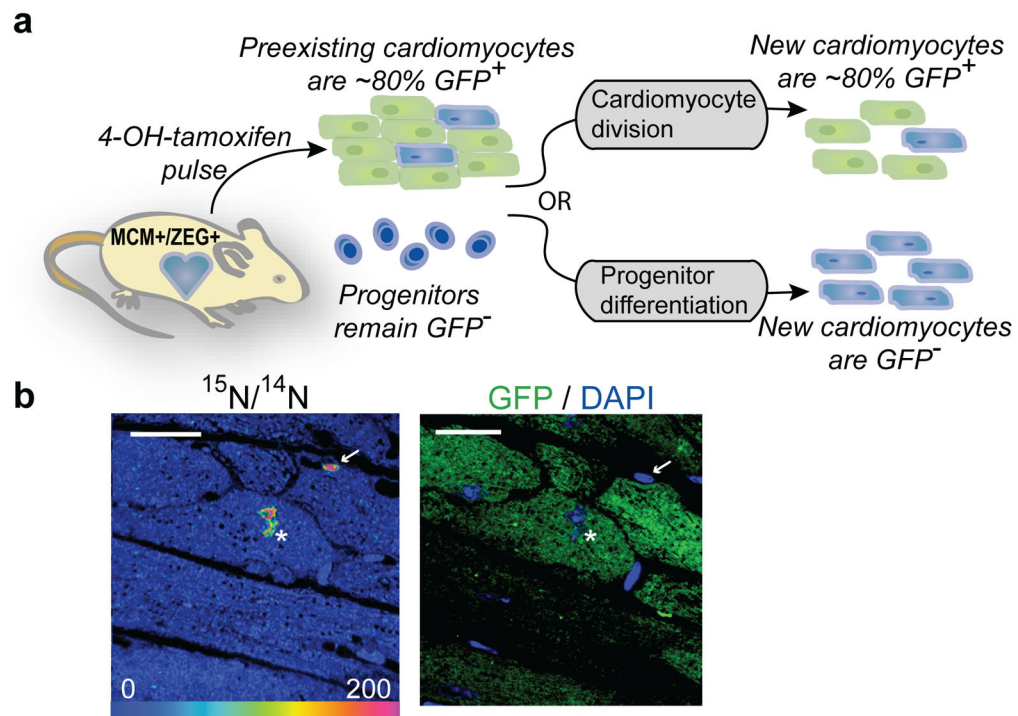
Figure 3. New cardiomyocytes are derived from pre-existing cardiomyocytes during aging

a) Experimental strategy. MerCreMer[+]/ZEG[+] mice (n=4) treated for 2 wks with 4OH-tamoxifen to induce cardiomyocyte-specific GFP expression. ^{15}N-thymidine administered continuously during 10 wk chase, then cycling cells identified by ^{15}N-labeling. New cardiomyocytes ([15]N[+]) derived from preexisting cardiomyocytes should express GFP at a rate similar to surrounding quiescent ([15]N[−]) cardiomyocytes. New cardiomyocytes ([15]N[+]) derived from progenitors should be GFP[−].

b) Left: [15]N:[14]N HSI image demonstrating ^{15}N-thymidine labeled cardiomyocyte nucleus (white asterisk) and ^{15}N-labeled non-cardiomyocyte (white arrow). Right: Immunofluorescent image showing ^{15}N-labeled cardiomyocyte is GFP[+]. Scale bar = 15μm.
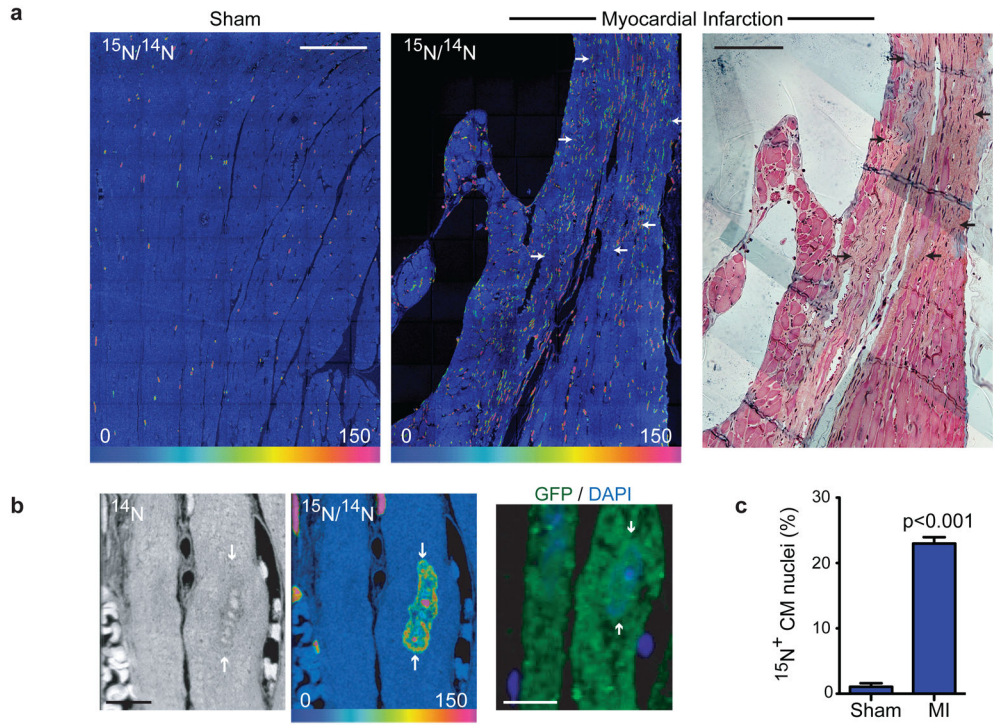
Figure 4. Myocardial injury stimulates division of pre-existing cardiomyocytes

a) Myocardial infarction (MI) leads to extensive DNA synthesis within and adjacent to scar (arrows). MerCreMer[+]/ZEG[+] mice were treated for 2 wks with 4OH-tamoxifen to induce cardiomyocyte-specific GFP expression before MI or sham surgery, then ^{15}N-thymidine administered continuously for 8wks. Mosaics of 70 60×60μm MIMS tiles. Trichrome stained adjacent section (far right) shows scar. Scale bars = 90μm.

b) ^{15}N-thymidine labeled cardiomyocyte nucleus (white arrows) from MI border region. Immunofluorescent staining demonstrates that the cardiomyocyte is GFP[+]. Scale bars = 10 μm.

c) Mean % ^{15}N[+] cardiomyocyte nuclei after MI (n=4) in the scar border region compared to sham operated mice (n=3). Mean% ± S.E.M.

Table 1

^{15}N-labeled cardiomyocytes (^{15}N$^+$ CM) during normal aging

Includes new mononucleated/diploid fraction, demonstrated a similar rate of GFP expression compared to background ^{15}N$^-$ cardiomyocytes.

	Total counted	GFP $^+$	% GFP $^+$
^{15}N$^-$ CM	1111	933	84%
^{15}N$^+$ CM	35	27	77%
Polyploid CM	12	10	83%
Diploid CM	22	17	77%
Multinucleated CM	18	14	78%
Mononucleated CM	17	14	82%
Diploid/Mono CM	6	5	83%

Table 2

GFP analysis of ^{15}N-labeled cardiomyocytes (^{15}N$^+$ CM)

Pooled analysis of 4 mice in MI group and 3 mice in sham group. MI led to dilution of GFP$^+$ cardiomyocytes adjacent to scar. New cardiomyocytes generated after MI (the ^{15}N$^+$/diploid/mononucleated pool) were predominantly GFP$^+$ consistent with division of preexisting cardiomyocytes.

	Total	GFP$^+$	% GFP$^+$
Sham	3411	2693	79%
^{15}N$^+$ CM	23	19	83%
MI	7063	4766	67%
^{15}N$^+$ CM	205	146	71%
PolyploidCM	126	97	77%
DiploidCM	65	47	72%
Multinucleated CM	59	42	71%
Mononucleated CM	41	29	71%
Diploid/MonoCM	16	11	69%